

Supplementary information for

Direct measurements of exciton diffusion length limitations on organic solar cell performance

Derek R. Kozub, Kiarash Vakhshouri, Sameer Vajjala Kesava, Cheng Wang, Alexander Hexemer, and Enrique D. Gomez*

1. Materials and Methods

Solutions of 1:4 by mass PBTTT ($M_n = 26$ kg/mol, polydispersity = 1.9, Merck) and PC₇₁BM (>99.5%, Nano-C) were made with anhydrous 1,2-dichlorobenzene (Sigma-Aldrich). Solutions were stirred for at least 1 hr at 100 °C prior to use to ensure dissolution and all solutions were made in a N₂ glovebox.

Conditions for TEM and GISAXS samples were made to closely match conditions relevant to organic solar cells. Thin films of PBTTT:PC₇₁BM were cast on 70 nm poly(3,4-ethylenedioxythiophene) poly(styrenesulfonate), PEDOT:PSS, (Clevios P, H.C. Starck) films deposited on silicon wafers. Silicon wafers were cleaned through sonication for 10 min in acetone and 10 min in isopropanol followed by 10 min of UV-ozone treatment. Thin films (ca. 42 ± 5 nm) for TEM experiments were made by spin coating 15 mg/mL solutions in a N₂ glove box at 1000 rpm for 1 min. Films were floated-off in filtered distilled water and placed on copper TEM grids. Samples were dried for 24 hrs under vacuum and annealed on a calibrated digital hot plate in a N₂ glove box. Films were rapidly cooled to room temperature after annealing was complete by placing them on a metal surface.

TEM experiments took place at the Materials Research Institute of the Pennsylvania State University on a JEOL 2010 LaB₆ and on a Zeiss LIBRA 200MC at the National Center for Electron Microscopy, Lawrence Berkeley National Laboratory. Bright field images, thickness maps and elemental maps were captured. Sulfur and carbon elemental maps were obtained through the standard three-window method. Domain compositions were estimated from the combination of elemental maps and thickness maps as described previously.¹ In order to convert mass fractions to volume fractions we assume the density of PBTTT is 1.1 g/cm³, similarly to P3HT. Our analysis is not sensitive to the density of PBTTT; variations in the density of 10% change our results within the error bars of our measurements.

Grazing Incidence Small Angle X-Ray Scattering (GISAXS) experiments were conducted on beamline 7.3.3 at the Advanced Light Source, Lawrence Berkeley National Laboratory ($\lambda = 1.24$ Å). In a similar manner as for TEM samples, PBTTT/PC₇₁BM thin films (ca. 70 ± 10 nm) were spun-cast on PEDOT:PSS/silicon substrates from 24 mg/mL solutions. Samples were annealed on PEDOT:PSS/silicon substrates inside a N₂ glove box. GISAXS data was taken at angles above the critical angle for 1:4 PBTTT/PC₇₁BM mixtures (0.14°) but below the silicon critical angle (0.21°). We focus on in-plane data at the specular reflection and assume

the Born Approximation is valid. Scattering data was corrected for scattering from air and the substrate as described in the Supporting Information of reference 1.

Solar cells (device area = 0.162 cm²) were fabricated on indium tin oxide (ITO) coated glass substrates (Kintec, Hong Kong). The substrates were cleaned with Aquet detergent solution and water, followed by 10 min of sonication in acetone and 10 min in isopropanol and 10 min of UV-ozone treatment. PEDOT:PSS was spun cast in a laminar flow hood at 4000 rpm for 2 min and subsequently dried at 165 °C for 10 min (thickness ca. 70 nm). PBTTT/PC₇₁BM (24 mg/mL, 70 ± 10 nm) active layers were spun cast in a N₂ glovebox at 1000 rpm for 1 min. A 75 nm layer of aluminum was deposited via thermal evaporation at 10⁻⁶ torr.

Electrical characterization of devices in the dark and under AM 1.5G (0.1 mW/cm²) illumination from a 150W Newport solar simulator was performed using a Keithley 2636A Sourcemeter. All devices testing took place in a N₂ glovebox. At least 6 devices were averaged for all of the data presented here.

2. EFTEM image analysis

We can estimate the compositions of the domains since the image intensities in Figure 1 are proportional to the concentration of sulfur.¹ In particular, we focus on films annealed at 150 °C for 5 min and 190 °C for 30 min because the clearly developed structures facilitate analysis of the domain intensities. The PC₇₁BM-rich regions are composed of 16 ± 3 % and 14 ± 2 % by volume PBTTT for films annealed at 150 °C for 5 min and 190 °C for 30 min, respectively. Thus, our results indicate that pure PC₇₁BM phases are not prevalent. Assuming that the width equals the depth at the center of each domain, we obtain that PBTTT-rich regions are composed of 64 ± 6 % PBTTT after annealing at 150 °C for 5 min. We also analyzed the intensity of the very bright regions, which we attribute to overlapping domains as mentioned in the main text. Assuming these very bright domains span the thickness of the film (42 nm), the composition of such films is 62 ± 3% PBTTT, consistent with our result for the rest of the light regions. Since the compositions are close to that of intercalated PBTTT/PC₇₁BM domains (40% PBTTT by mass² and 48% PBTTT by volume), we conclude that the light regions are composed of intercalated PBTTT/PC₇₁BM with some pure PBTTT or PC₇₁BM-depleted regions.

For films annealed at 190 °C for 30 min, domain sizes are mostly larger than the film thickness (ca. 40 nm). We assume that the domains span the thickness of the film and obtain the composition of the PBTTT-rich domains to be 42 ± 4 %. Within each of the PBTTT domains 20 nm rod-like features are visible; the darker regions contain 36 % while the lighter regions contain 48 % PBTTT. Therefore, we attribute the majority of the light regions to be composed of intercalated co-crystals of PBTTT/PC₇₁BM, while the dark regions within PBTTT-rich domains to be either partially intercalated or distinct PC₇₁BM domains.

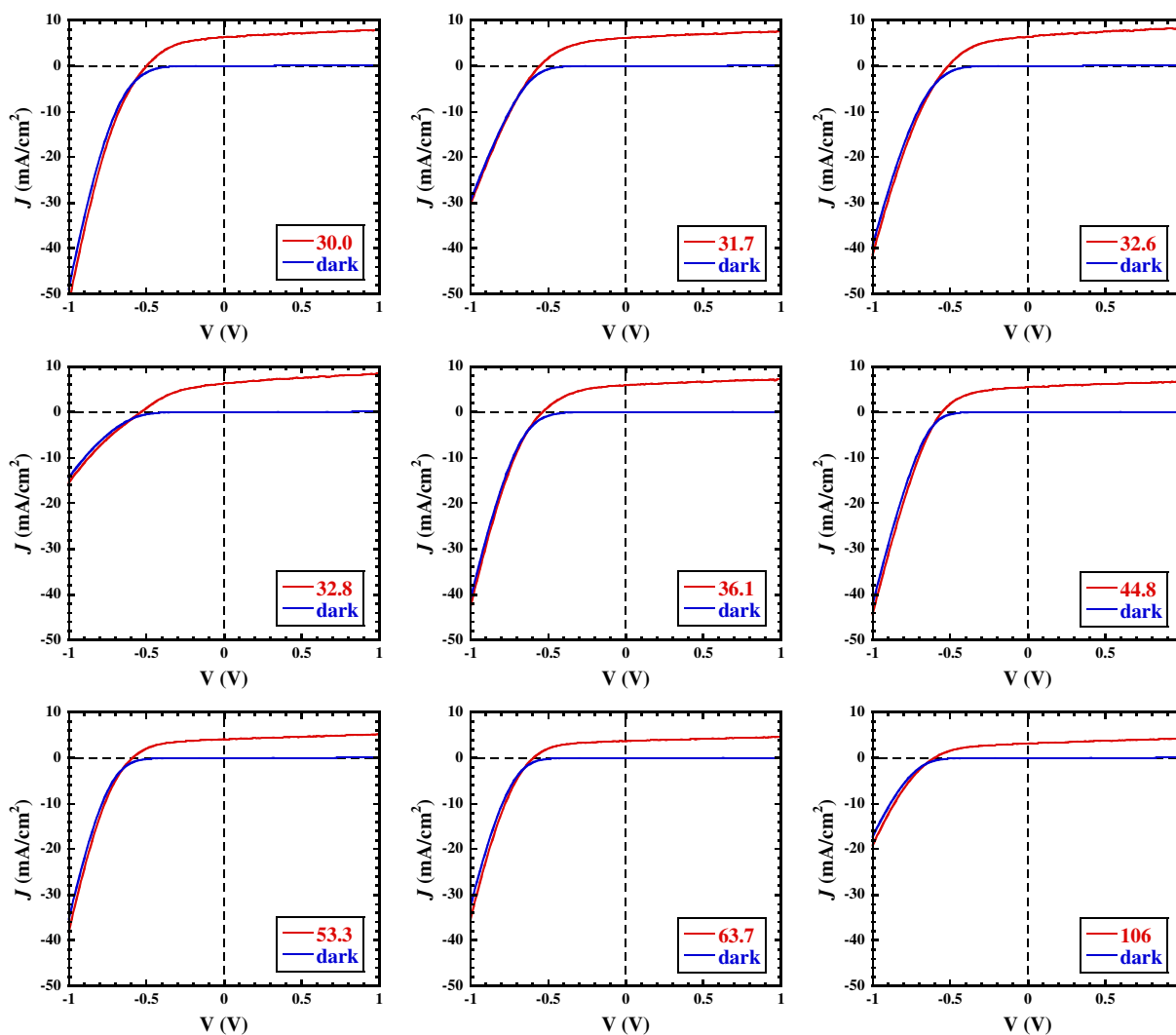


Figure S1. J-V characteristics of representative 1:4 PBTBT/PC₇₁BM devices under illumination and in the dark. Graphs are labeled in terms of the domain spacing (in nm) obtained from GISAXS.

3. PBTBT/PC₇₁BM device data and analysis

From Figure 1 of the main text and the discussion in the previous section, it is apparent that domain continuity may be compromised for some of the processing conditions of this study. Further examination of the characteristic J-V curves of PBTBT/PC₇₁BM devices, shown in Figure S1, demonstrates that the current at forward bias (-1 V) varies with processing conditions. The lower currents at -1 V for devices with an active layer domain spacing of 32.8 or 106 nm suggest that the series resistance is higher for these devices. Furthermore, Figure S2 shows that the fill factor varies from 0.42 to 0.52 for devices in this study, also suggesting that the charge extraction efficiency varies with processing conditions and morphology.

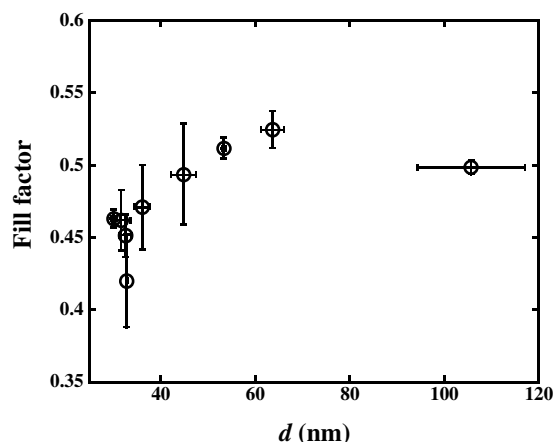


Figure S2. Fill factor as a function of d-spacing obtained from GISAXS. Error bars are the standard deviation of multiple measurements.

We explore the consequence of a varying series resistance on our device characteristics using the standard equivalent circuit model for solar cells,³ as shown in Figure S3. Increasing the series resistance decreases the current at forward bias (-1 V) and eventually decreases both the fill factor and short-circuit current (J_{SC}). Note that no other parameters were varied to obtain the results in Figure 3. However, until the series resistance becomes very large, such that almost no photovoltaic or diode characteristics are apparent, the current at reverse bias (1 V) remains largely unchanged. The applied field overcomes the effect of the enhanced series resistance, such that the current at reverse bias approaches the photogenerated current. Thus, J at reverse bias is a more robust estimate of the photogenerated current of the cell than J_{SC} , since it is less susceptible to charge transport limitations.

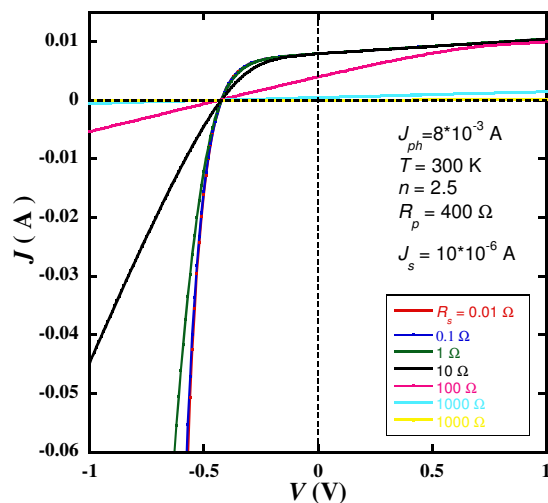


Figure S3. Simulated J-V curves from the equivalent circuit model for photovoltaics³ as a function of increasing series resistance (R_s). Note that as R_s increases, the fill factor decreases and the short-circuit current also decreases. The current at reverse bias (1 V), however, does not change significantly with R_s until R_s is very large and diode characteristics are not apparent.

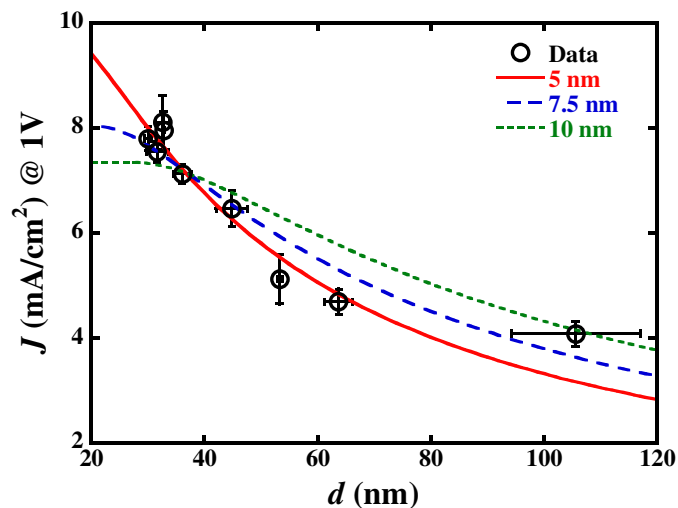


Figure S4. Current at reverse bias ($J @ 1V$) vs. d -spacing obtained from GISAXS. The curves are estimates of J using a morphological model described in the main text. Model results are shown for different exciton diffusion lengths (5 nm, 7.5 nm, 10 nm). Error bars denote the standard deviation of multiple measurements.

Figure S4 shows the current at reverse bias versus d -spacing from GISAXS. The curves are generated using the morphological model described in the text and various exciton diffusion lengths. Our simple model does not account for charge transport limitations; consequently, Figure S4 (which utilizes $J @ 1V$ to describe device performance) should provide better agreement between the model and experiment than Figure 3b of the main text. Comparison of the two graphs, however, demonstrates that the fits are adequate for both Figure S4 and Figure 3b of the main text. Thus, the charge extraction efficacy is sufficiently invariant between devices to enable the prediction of the J_{SC} from GISAXS morphological data using the exciton diffusion length.

Table S1 provides a summary of the device data obtained from this study.

Table S1. Summary of 1:4 PBTTT/PC₇₁BM device data

Thermal annealing conditions	Domain spacing (<i>d</i>), GISAXS (nm)	Efficiency (%)	<i>V</i> _{oc} (V)	FF	<i>J</i> _{sc} (mA/cm ²)	<i>J</i> @ 1 V (mA/cm ²)
As-cast	32.8±0.1	1.4±0.2	0.52±0.03	0.42±0.03	6.2±0.1	8.0±0.4
125 °C 10 min	32.6±1.2	1.5±0.1	0.52±0.01	0.45±0.01	6.3±0.4	8.1±0.5
125 °C 30 min	30.0±0.6	1.5±0.1	0.53±0.02	0.46±0.01	6.3±0.1	7.8±0.2
150 °C 2 min	31.7±1.9	1.5±0.1	0.55±0.02	0.46±0.02	6.1±0.1	7.5±0.2
150 °C 10 min	36.1±1.6	1.5±0.1	0.56±0.01	0.47±0.03	5.8±0.2	7.1±0.2
150 °C 30 min	44.8±2.7	1.5±0.1	0.56±0.01	0.49±0.03	5.4±0.2	6.5±0.3
190 °C 2 min	53.3±0.4	1.2±0.08	0.59±0.01	0.51±0.01	4.1±0.4	5.1±0.5
190 °C 10 min	63.7±2.4	1.2±0.03	0.60±0.01	0.52±0.01	3.7±0.1	4.7±0.2
190 °C 30 min	106±11	0.93±0.04	0.60±0.01	0.50±0.01	3.1±0.2	4.1±0.2

References

1. D. R. Kozub, K. Vakhshouri, L. M. Orme, C. Wang, A. Hexemer and E. D. Gomez, *Macromolecules*, 2011, **44**, 5722-5726.
2. N. C. Miller, R. Gysel, C. E. Miller, E. Verploegen, Z. Beiley, M. Heeney, I. McCulloch, Z. N. Bao, M. F. Toney and M. D. McGehee, *Journal of Polymer Science Part B-Polymer Physics*, 2011, **49**, 499-503.
3. S. Yoo, B. Domercq and B. Kippelen, *Journal of Applied Physics*, 2005, **97**, 103706.